

Abstract

In this study, experimental and numerical analyses were carried out for determination of cohesion values of different types of rock materials using double shear jaws (DSJ) which can be practically used with the conventional compressive test equipment, to make shear planes in the rock core specimens. Effects of various parameters like jaw dimensions, gaps between triple blocks of the DSJ and contact conditions of the jaw on the results and validity of the cohesion test were investigated considering failure mechanisms of rock core specimens. Instead of a failure induced due to the shear stresses, tensile failures are mostly seen from conventional shear testing conditions. For a valid failure under the control of shear stresses, a DSJ design was suggested to be used in cohesion determination tests according to the results obtained from this study.

Keywords

shear strength of rock materials, cohesion, rock testing, experimental rock mechanics

1 Introduction

Although shear strength of rock materials is an important parameter for many different rock engineering applications, there is still a necessity for development of a standard method and details for determination of shear strength of rock materials. The conventional direct shear strength (DSS) test method suggested by International Society for Rock Mechanics and Rock Engineering (ISRM) and standards like ASTM D5607 are not a proper way to test high strength rock materials because of possible failure of cement mortar instead of rock core specimens [1–3]. The cement moulding method to hold specimens is more suitable for testing rock joints rather than intact rock materials. As another topic, the conventional DSS test has additional problems of impracticality in specimen preparation process including two steps cement mortar casting as seen in Fig 1. In this study, a practical test method for determination of cohesion values of rock materials is investigated to assess whether accurate strength values can be measured using double shear jaw (DSJ) which is a basic apparatus to test numerous specimens instead of only one specimen as in cement moulding method of holding. Within this purpose, new steel jaws for testing cohesion of rock materials were designed and manufactured in this study.

Need for waiting the curing time of several days for holding specimens in the casted mortar method should be stated as another disadvantage of the conventional DSS test. As an important issue which prevents to measure the strength value under pure shearing, significant bending/tension effect is induced as the rock specimen loaded in the soft cement mortar. Having the bending effect in the specimen causes to measure smaller strength values than that determined under pure shearing condition [4–7]. In this study, a new method of using DSJ was investigated for the aim of having ideal loading condition. For the conventional DSS equipment in rock mechanics laboratories, manual load application by using the hydraulic jack is an additional lacking to cause a personal effect on the strength results. On the other hand, double shear jaws (DSJs) let specimens to be loaded vertically with a constant rate which can be supplied by the load controlled compressive equipment.

¹ Department of Civil Engineering
Faculty of Engineering,
Giresun University
28200, Güre, Giresun, Turkey

² Department of Civil Engineering,
Faculty of Engineering,
Karadeniz Technical University,
61080, Ortahisar, Trabzon, Turkey

* Corresponding author, email: erenkomurlu@gmail.com

Use of steel shear jaws was thought to minimize the bending effect since a rigid surface would supply a limitation in deformation at specimen and jaw contact zone [8,9]. As another important problem for shear strength determination by holding specimens in the casted cement mortar, height of the mortar cannot be regulated precisely and gap dimension between the two step casted cement mortars varies in accordance with different reasons such as manual casting details, consolidation, evaporation, cement type, water content and etc. Because of varying gap distance between up and down side cement parts, results can be personalized in the conventional DSS test. On the other hand, a constant distance between the opposite forces supplying the shear effect is easy to be made using DSJs.

In this study, the results obtained with newly investigated shear strength test jaws and validity of failure observed for different test details are investigated to assess whether the double shear jaw (DSJ) can be used to accurately evaluate the cohesion values of rock materials. Additionally, a series of numerical analyses was carried out to compare its results with those obtained from the experimental study and to investigate stress distribution in the core specimens loaded by the DSJs for determination of the ideal failure shape and jaw dimensions.

2 Experimental study

2.1 Materials and method

A series of shear strength tests was applied on limestone, tuff, andesite, dacite and marble type five different rock materials by using double shear jaws (DSJs) consisting of three drilled steel blocks with inner diameter of 54.5 mm and 53.5 mm. As given in Fig. 2 that shows dimensions of the jaws manufactured, steel blocks with the size of 150 mm × 100 mm × 100 mm were drilled and cut into three pieces to create the shear effect. Two jaws with different drill diameters of 54.5 mm and 53.5 mm were manufactured to prevent gap occurrence between rock core specimen and steel drill surface. The

drill diameters of jaws were chosen to fit well with specimens cored by NX size (54.7 mm) drill bit which was used in this study. As a result of abrasion during the coring process, specimen diameters changed depending upon the material type. As an example, tuff specimens diameter decreased to 53 mm because of its high abrasion resulting from the soft material property. The gap between jaw drills and specimens was no more than 1 mm for all specimens tested in this study.

Loading rate was chosen to be 0.2 kN/sec in the DSJ test. A sensitive hydraulic loading press with the load capacity of 300 kN was used in the experimental study (Fig. 3). Changes of two different variables of gap between steel pieces of the jaw (*a*) and length of the middle piece block (*b*) were investigated to evaluate the effect of those dimensional parameters on the results and failure mechanisms. To manufacture the jaws used in this study, *b* variable was chosen in accordance with the numerical analyses to have an enough distance between two shear planes for having no stress effect on each other. Four different *a* values of 0 mm, 3 mm, 6 mm and 9 mm and *b* value of 60 mm were tested in the experimental study. After inserting the rock cores cut with the length of 150 mm into the drills of jaws, the middle blocks were rotated with 180° to make the ability of loading specimens (Fig. 3). As the specimens loaded by the hydraulic press, right and left side parts of the jaw made two couples of shear forces.

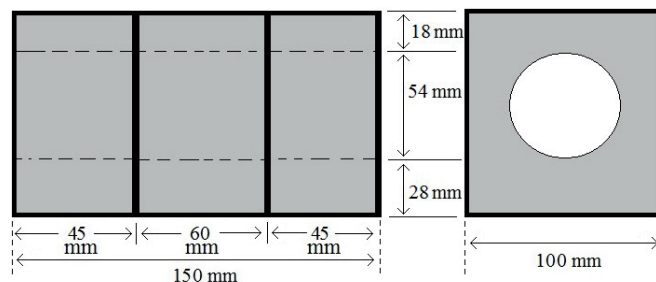


Fig. 2 Double shear jaw dimensions



Fig. 1 a) Moulding in conventional shear strength test, b and c) Loading equipment, d) a failed specimen



Fig. 3 Double shear jaw under loading

Additional tests were carried out to investigate the effect of contact angle (α) of the middle block, As seen in Fig. 4, middle blocks with the contact angles of 15° were manufactured and tested in addition to the fully contacted specimens loaded under the jaws with untreated drill holes ($\alpha:180^\circ$). The contact angle of the treated jaws was selected in accordance with the results obtained from the numerical modelling study. The details for selection of the contact angle can be found in the numerical modelling part of this study.

2.2 Results

The failure loads obtained with DSJ tests are given in Table 1. According to the results, failure load for all tested rock materials was found to decrease with an increase in a value. Significant changes in the failure shapes of the specimens were observed under the loading conditions of varying a values. As seen in Fig. 5, deviated cracks and angular failure surfaces were observed from the tests applied in the case of high a values, whereas vertical and ideal shearing plane cracks which are parallel to the loading direction were seen under the loading condition of $a = 3$ mm. On the other hand, crushing zone at the contact and frequent cracks were seen in tests under the condition of $a = 0$ mm (Fig. 6). The high load values, frequent cracks and crumbled crushing zone occurrence indicate the unnecessary and misleadingly high energy consumption for failure, which causes to calculate high strength values for the condition of $a = 0$ mm. With an increase

in a value from 3 mm, crack inclination was seen to start. Especially, cracks were found to be highly deviated from the shear forces direction under the loading condition of $a = 9$ mm (Fig. 5c and Fig 5d). Some crack shapes under the condition of $a = 6$ mm are given in Fig. 7 ($\alpha:180^\circ$).

15° contact jaws were only tested for the condition of $a = 3$ mm because of determination as the most ideal gap dimension from the ideal failure shape. Cracking shape under the treated jaws with 15° contact angle was found similar with that observed from the loading under the untreated jaw with the case of $a = 3$ mm. As same with the fully contacted specimens under the untreated jaws, simple crack shapes parallel to the loading direction were seen under the 15° jaws ($a = 3$ mm). As only difference between treated and untreated jaws, a typical and minor local spalling zone just beneath the edge of the treated middle DSJ block where is the location of the crack initiation was occurred in case of testing under 15° contact angle. Higher failure loads were obtained from the fully contacted specimens in comparison with the specimens loaded under the treated jaws (Table 1).

Failure shapes obtained from the case of $a = 0$ mm and full contact condition can be easily designated from the major crushing parts (Fig. 6). On the other hand, there was no cracking in left and right side blocks under the 15° jaw ($a = 3$ mm). As stated above, the location to initiate failure under the 15° jaw was beneath the treated hole edge of the middle block. The failure

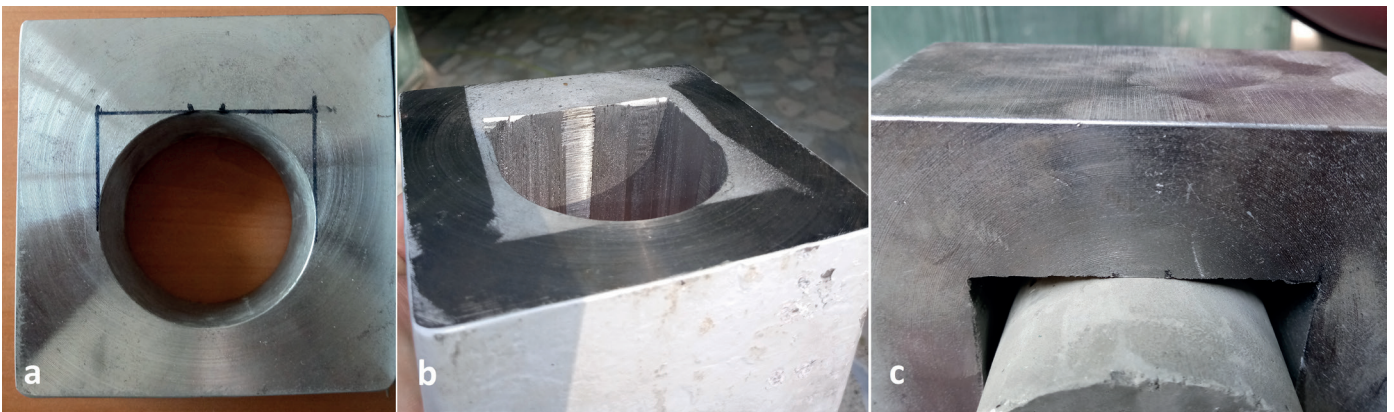


Fig. 4 a) A full contact drill and cutting design of 15° jaw, b) treated hole with 15° contact angle, c) a specimen contact in the treated middle block of 15° jaw

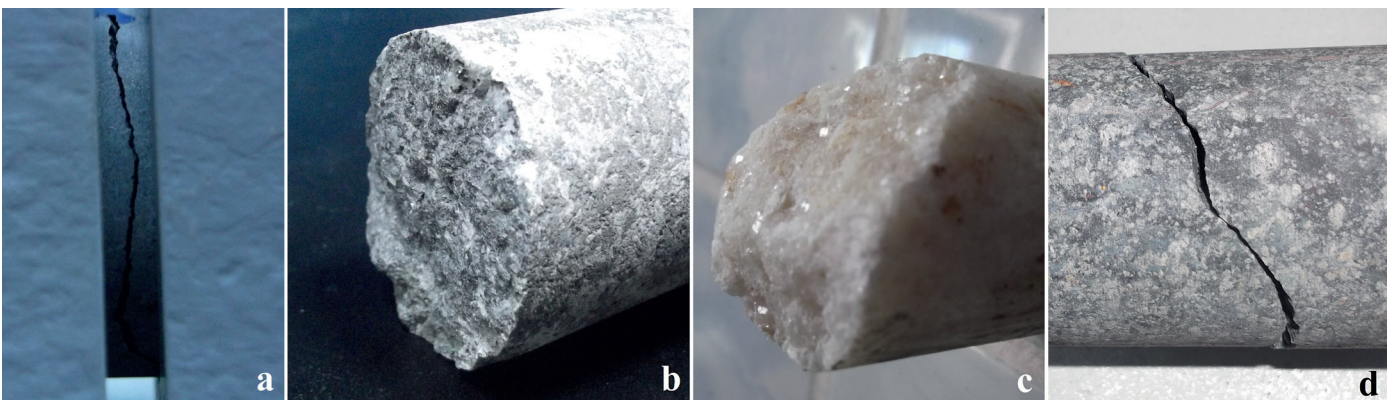
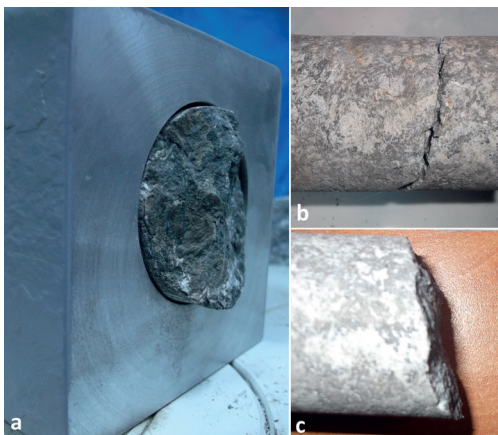


Fig. 5 Failed specimens in untreated full contact drill ($\alpha:180^\circ$) and under the loading conditions of $a = 3$ mm and $b = 60$ mm (a, b), $a = 9$ mm and $b = 60$ mm (c, d)

Table 1 Failure loads measured from experimental study (S.D.: Standard deviation, $\alpha:180^\circ$ is full contact condition, α :contact angle)

Loading Condition	Rock Type	Failure Load (kN)	Specimen number	S.D. (kN)
$a: 0 \text{ mm}, b: 60 \text{ mm} (\alpha:180^\circ)$	Limestone	11.2	3	0.6
$a: 3 \text{ mm}, b: 60 \text{ mm} (\alpha:180^\circ)$	Limestone	10.3	3	0.7
$a: 6 \text{ mm}, b: 60 \text{ mm} (\alpha:180^\circ)$	Limestone	9.1	3	0.5
$a: 9 \text{ mm}, b: 60 \text{ mm} (\alpha:180^\circ)$	Limestone	8.0	3	0.7
$a: 0 \text{ mm}, b: 60 \text{ mm} (\alpha:180^\circ)$	Tuff	6.3	3	0.4
$a: 3 \text{ mm}, b: 60 \text{ mm} (\alpha:180^\circ)$	Tuff	5.5	3	0.5
$a: 6 \text{ mm}, b: 60 \text{ mm} (\alpha:180^\circ)$	Tuff	4.4	3	0.3
$a: 9 \text{ mm}, b: 60 \text{ mm} (\alpha:180^\circ)$	Tuff	3.2	3	0.4
$a: 0 \text{ mm}, b: 60 \text{ mm} (\alpha:180^\circ)$	Andesite	15.7	3	0.8
$a: 3 \text{ mm}, b: 60 \text{ mm} (\alpha:180^\circ)$	Andesite	14.0	3	1.0
$a: 6 \text{ mm}, b: 60 \text{ mm} (\alpha:180^\circ)$	Andesite	12.1	3	0.9
$a: 9 \text{ mm}, b: 60 \text{ mm} (\alpha:180^\circ)$	Andesite	9.8	3	0.6
$a: 0 \text{ mm}, b: 60 \text{ mm} (\alpha:180^\circ)$	Marble	12.4	3	0.5
$a: 3 \text{ mm}, b: 60 \text{ mm} (\alpha:180^\circ)$	Marble	11.3	3	0.7
$a: 6 \text{ mm}, b: 60 \text{ mm} (\alpha:180^\circ)$	Marble	9.9	3	0.9
$a: 9 \text{ mm}, b: 60 \text{ mm} (\alpha:180^\circ)$	Marble	8.6	3	0.8
$a: 3 \text{ mm}, b: 60 \text{ mm} (\alpha:180^\circ)$	Dacite	18.6	3	0.9
$a: 3 \text{ mm}, b: 60 \text{ mm} (\alpha:15^\circ)$	Dacite	16.5	3	1.0
$a: 3 \text{ mm}, b: 60 \text{ mm} (\alpha:15^\circ)$	Limestone	8.9	3	0.4
$a: 3 \text{ mm}, b: 60 \text{ mm} (\alpha:15^\circ)$	Andesite	12.7	3	0.5

**Fig. 6** Failure under the loading condition of $a = 0 \text{ mm}$ and $b = 60 \text{ mm}$ ($\alpha = 180^\circ$)**Fig. 7** Failure under the loading condition of $a = 6 \text{ mm}$ and $b = 60 \text{ mm}$

occurred with a single and vertical shear plane crack under 15° jaw is shown in Fig. 8. Reasons for various crack initiation parts under different jaws and loading conditions were investigated with the numerical analyses as given in the following part.

3 Numerical study

3.1 Model properties and methodology

Reasons for having different failure shapes and failure mechanisms of the shear test specimens were investigated with a series numerical modelling analyses. To better understand the stress distributions under different loading conditions, Finite Element Analyses (FEM) were performed by using the ANSYS software. In the numerical study, four different a values of 0 mm, 3 mm, 6 mm and 9 mm were investigated as same in the experimental study. Additionally, three different jaws with varying b values of 20 mm, 60 mm and 100 mm were analysed to understand which length of the middle block is enough. Some different jaw and rock core models are seen in Fig. 9. Material properties as input values for jaw steel and rock core specimen models are given in Table 2. As core specimens and drill of the jaw were modelled to

Table 2 Material properties as input values

Parameter	Rock	Steel
Compressive Strength	60 MPa	300 MPa
Tensile Strength	5 MPa	250 MPa
Modulus of Elasticity	30 GPa	200 GPa
Poisson's Ratio	0.25	0.30
Cohesion (Shear Strength)	6 MPa	250 MPa

have the same diameter of 54 mm, rock core and jaw models were contacted in numerical analyses. The contact surfaces between the rock and loading apparatus were simulated with the Conta174 and Targe170 contact pairs. The friction coefficient between rock and steel of the loading jaw was considered as 0.3 for all analyses.

Eight-node solid brick elements (Solid65) were used for three-dimensional modelling of rocks, which have the capability of cracking in tension, crushing in compression, plastic deformation, and three degrees of freedom at each node, including transition in the nodal x, y, and z directions. Materials were modelled by considering the linear and non-linear properties defining the behaviors of the elements. The modulus of elasticity in models was assumed same for tension and compression. The modelled material was defined as linear elastic material until the crack initiation occurs. After the crack initiation, change of the normal and shear stresses has been re-calculated by the program. The re-calculated shear stresses were transferred by the plasticity due to the generated open and closed cracks. The shear transfer coefficient was accepted as 0.3 and 0.1 for closed and open cracks, respectively. In addition, the

stiffness reduction factor considered as 0.6 to define plasticity had an important role in the behaviour of cracked elements.

These models predicted the failure of brittle materials according to the Willam–Warnke failure criteria used for concrete, rocks and other cohesive–frictional materials such as ceramics [10]. Material of the loading apparatus was modelled with Solid185 as a steel material with 200 GPa modulus of elasticity. A static analysis was performed for each of the models, and the full Newton–Raphson method was used for non-linear analysis. For displacement-controlled loading, loads were divided into multiple sub-steps until the total load was achieved. Stress distributions and cracking mechanisms for all specimen models were plotted for comparison with the experimental results.

The core rock specimen models had the length to diameter ratios of 2.1, 2.9 and 3.6 for *b* values of 20 mm, 60 mm and 100 mm, respectively. The mesh length in the rock models was chosen to be 1 mm. Several representative figures for various loading conditions are given in Fig. 9. As same in the experimental study, right and left side blocks of the three piece steel shearing jaw were modelled to have the length of 45 mm.

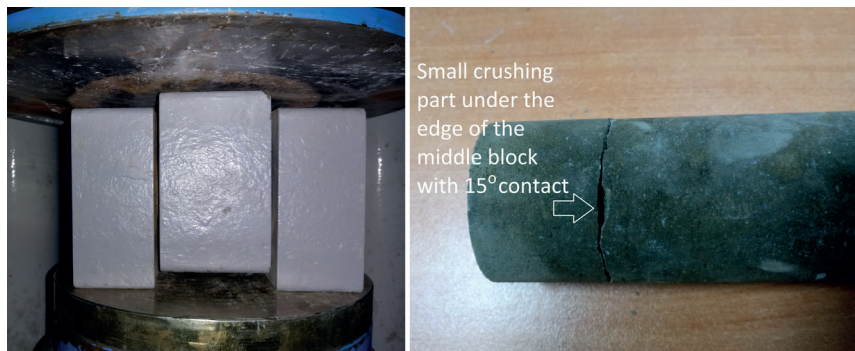


Fig. 8 a) Specimen loading, b) a failed specimen with minor crushing (spalling) under 15° jaw and *a* = 3mm condition

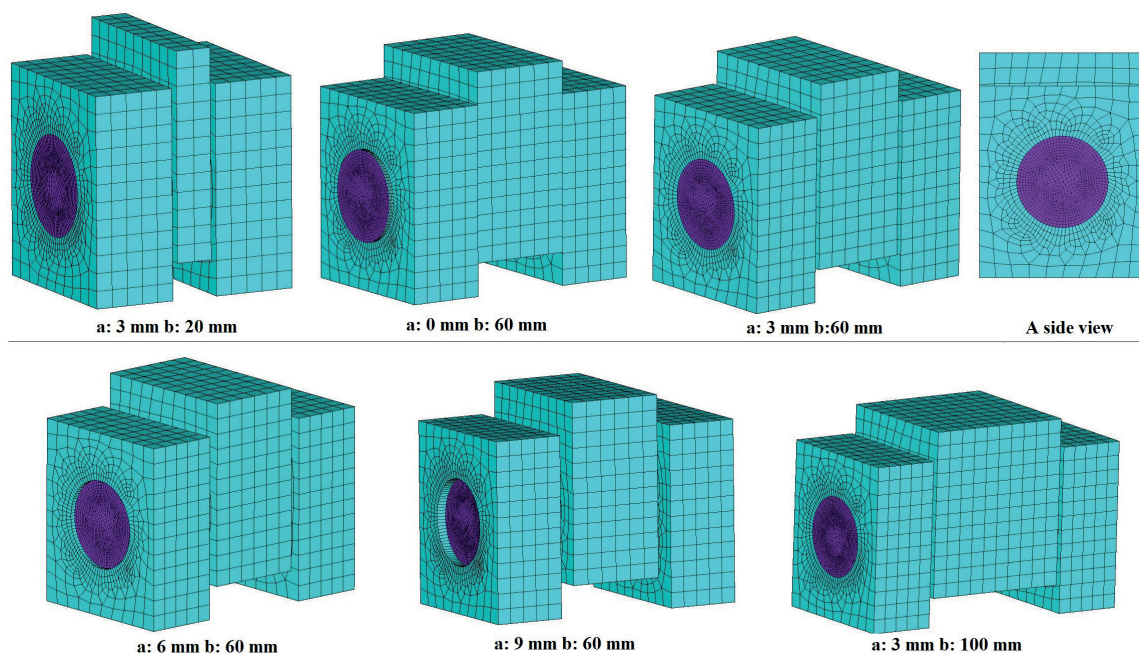


Fig. 9 Different numerical models

Load contact angle was another parameter to be investigated in the numerical modelling study. In addition to fully contacted specimens in the untreated hole, different contact angles of 65°, 45°, 25° and 15° were analysed modelling treated holes of the middle blocks of DSJs (Fig. 10). The jaw models with treated holes ($a = 65^\circ$, $a = 45^\circ$, $a = 25^\circ$, $a = 15^\circ$) respectively have a and b values of 3 mm and 60 mm. In this study, stress distributions, failure mechanisms and crack shapes of the core specimen models were investigated for different

contact angles. The reason for modelling different contact angles is making different shear stress concentrations in specimens as seen in the following results part.

3.2 Results

Several representative figures for stress distributions under various loading conditions are given in Figs. 11–13. To clarify the crack initiation of models shown in the figures, stresses at critical locations of maximum tension and maximum shear are

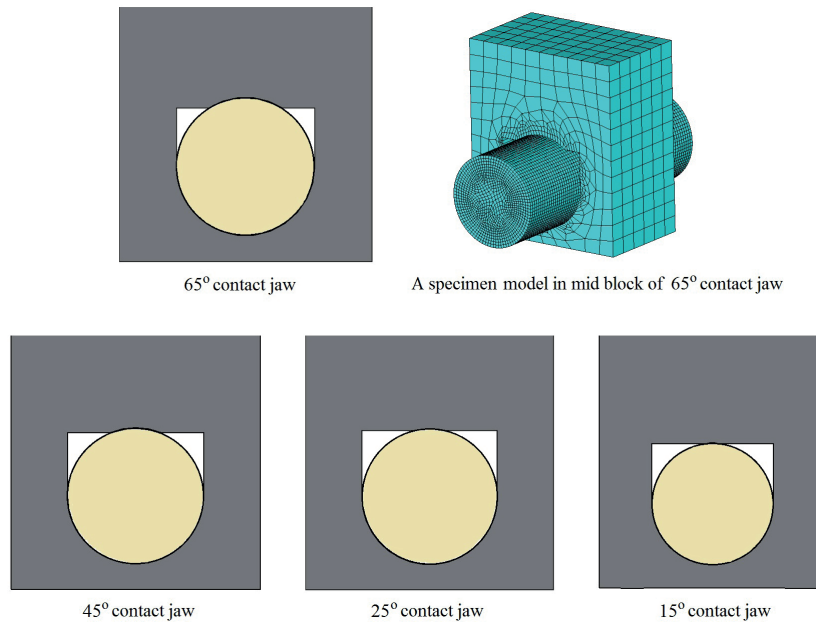


Fig. 10 Drill designs for various contact angles

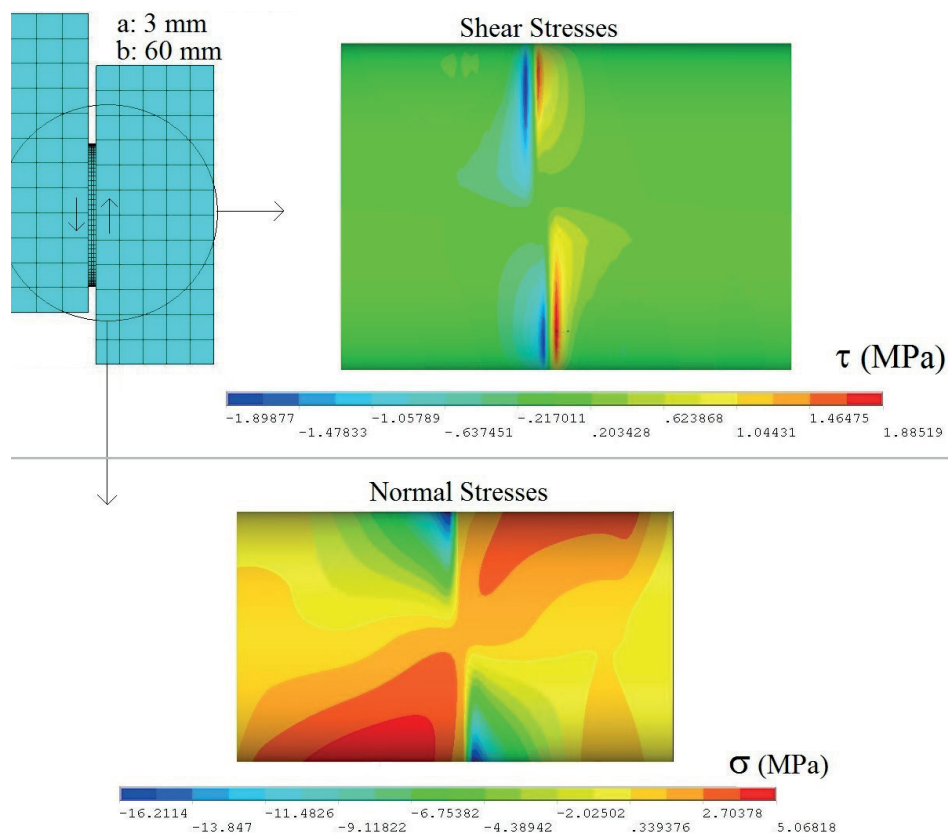


Fig. 11 Stress distribution in the model under the loading condition of $a = 3$ mm and $b = 60$ mm ($\alpha = 180^\circ$)

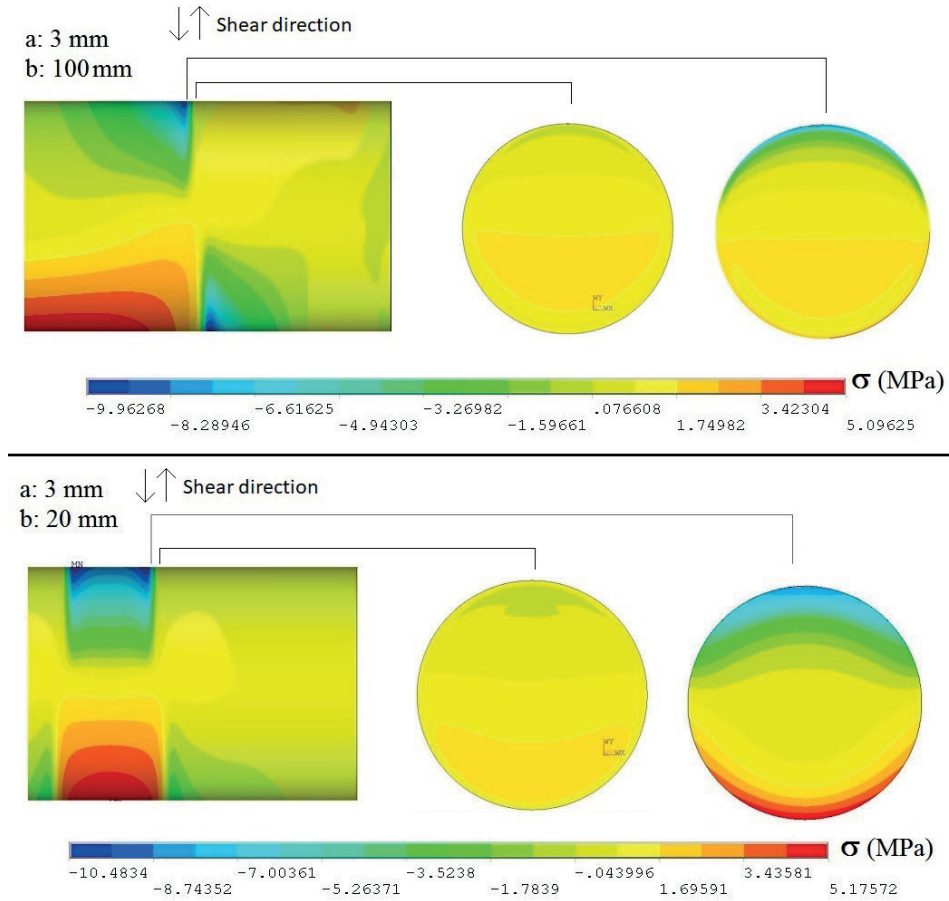


Fig. 12 Stress distribution in the model with the a value of 3 mm under the loading conditions of $\alpha = 180^\circ$, $b = 100$ mm (up) and $b = 20$ mm (down)

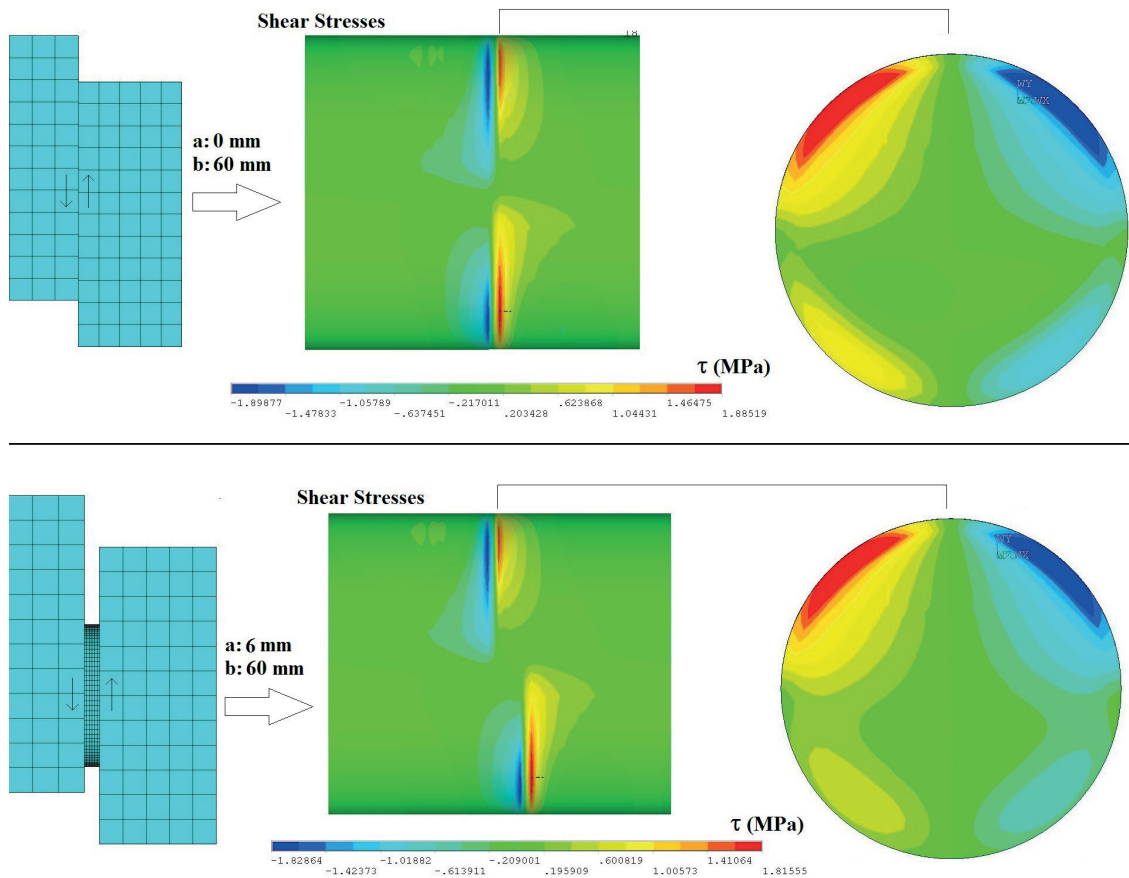


Fig. 13 Shear stress distribution in the model with a value of 60 mm under the loading conditions of $\alpha = 180^\circ$, $a = 0$ mm (up) and $a = 6$ mm (down)

Table 3 Stresses at critical locations of maximum tension and shear ($\alpha:180^\circ$)

Loading Condition	Max. Shear Stress, τ_{\max} (MPa)	Tension at max. shear location, σ_t (MPa)	Max. Tensile Stress, σ_{\max} (MPa)	Shear at Maximum tension location, τ (MPa)
$a: 3 \text{ mm}, b: 20 \text{ mm}$	1.17	3.14	5.20	0.13
$a: 3 \text{ mm}, b: 100 \text{ mm}$	1.95	3.42	5.09	0.50
$a: 0 \text{ mm}, b: 60 \text{ mm}$	1.91	3.71	4.88	0.43
$a: 3 \text{ mm}, b: 60 \text{ mm}$	1.89	3.89	5.07	0.63
$a: 6 \text{ mm}, b: 60 \text{ mm}$	1.82	3.98	5.15	0.33
$a: 9 \text{ mm}, b: 60 \text{ mm}$	1.72	4.55	5.70	0.19

Table 4 Maximum loads and failure mechanisms of the models

Loading Condition	Maximum Load (kN)	Failure Mechanism
$a: 3 \text{ mm}, b: 20 \text{ mm} (\alpha:180^\circ)$	8.91	Tensile stress induced
$a: 3 \text{ mm}, b: 100 \text{ mm} (\alpha:180^\circ)$	10.34	Tensile stress induced
$a: 0 \text{ mm}, b: 60 \text{ mm} (\alpha:180^\circ)$	10.80	Tensile stress induced
$a: 3 \text{ mm}, b: 60 \text{ mm} (\alpha:180^\circ)$	9.57	Tensile stress induced
$a: 6 \text{ mm}, b: 60 \text{ mm} (\alpha:180^\circ)$	8.59	Tensile stress induced
$a: 9 \text{ mm}, b: 60 \text{ mm} (\alpha:180^\circ)$	7.26	Tensile stress induced
$a: 3 \text{ mm}, b: 60 \text{ mm} (\alpha:65^\circ)$	9.12	Tensile stress induced
$a: 3 \text{ mm}, b: 60 \text{ mm} (\alpha:45^\circ)$	7.63	Tensile stress induced
$a: 3 \text{ mm}, b: 60 \text{ mm} (\alpha:25^\circ)$	6.76	Tensile stress induced
$a: 3 \text{ mm}, b: 60 \text{ mm} (\alpha:15^\circ)$	8.79	Shear stress induced

Table 5 Stresses at critical locations of maximum tension and shear

Loading Condition	Max. Shear Stress, τ_{\max} (MPa)	Tension at max. shear location (σ_t)	Max. Tensile Stress, σ_{\max} (MPa)	Shear at Maximum tension location (τ)
$a: 3 \text{ mm}, b: 60 \text{ mm} (\alpha:65^\circ)$	1.94	No tension	5.06	No shear
$a: 3 \text{ mm}, b: 60 \text{ mm} (\alpha:45^\circ)$	2.59	No tension	4.98	No shear
$a: 3 \text{ mm}, b: 60 \text{ mm} (\alpha:25^\circ)$	3.69	No tension	6.06	No shear
$a: 0 \text{ mm}, b: 60 \text{ mm} (\alpha:15^\circ)$	6.33	No tension	4.61	No shear

given in Table 3. All of the fully contacted rock models loaded in the untreated hole began to crack under the control of tensile stresses instead of shear stresses. It was found that tensile stresses maximize near the down side edges of the drill in the middle block of DSJ.

It was seen from the model with b value of 20 mm that the normal stresses are more dominant in comparison with the conditions of b value of 60 mm and 100 mm. Because of having small distance between right and left side shear planes, a relatively small failure load was obtained under the loading condition of $b = 20$ mm. There was no significant difference between shear stresses induced under the conditions of b values of 60 mm and 100 mm (Table 3). Because stress distributions in the critical parts are similar in cases of two different b values of 60 mm and 100 mm, it is inferred that 60 mm is acceptable as enough length of the middle block. Also, similar failure loads obtained from models with two different b values of 60 mm and 100 mm confirm that 60 mm is proper for having no need for higher middle block lengths (Table 4).

In fully contacted specimens, the shear stresses were found notably lower than tensile stresses. To increase the ratio of shear stresses to tensile stresses compared to those in the use of untreated drill holes making the full contact, different contact

angles of 65° , 45° , 25° , 15° were modelled as seen in Fig. 10. Stress distributions in the models with treated holes are given in Table 5. Additionally, stress distributions of some models are given in Figs. 14–16 ($a = 3$ mm, $b = 60$ mm). The decrease in contact angle was found to increase compressive stresses and shear stresses which were higher than tensile stresses and able to start cracking in the models with the contact angle of 15° and $a = 3$ mm condition. As seen from figures for the loading condition of the contact angle of 15° (Figs. 8 and 16), the maximum shear stress concentration location in the numerical analysis was confirmative for the cracking shape observed in the experimental study.

In case of excessive small contact angles, compressive stresses can be significant to cause a failure under the control of normal stresses. However, it was inferred from the numerical modelling results that 15° contact angle is not small enough for a failure started by the compressive stresses, considering the ratio of maximum compressive stress to maximum tensile stress of 4.2 which is a small ratio in comparison with typical relations between the compressive and tensile strength values of rock materials. Maximum compressive stress levels of different models are given in Table 6.

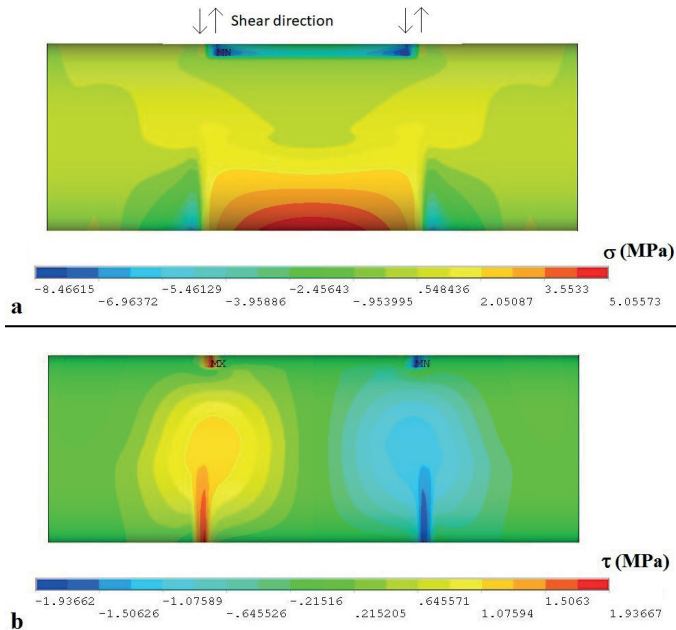


Fig. 14 Normal stress (a) and shear stress (a) distributions under 65° jaw

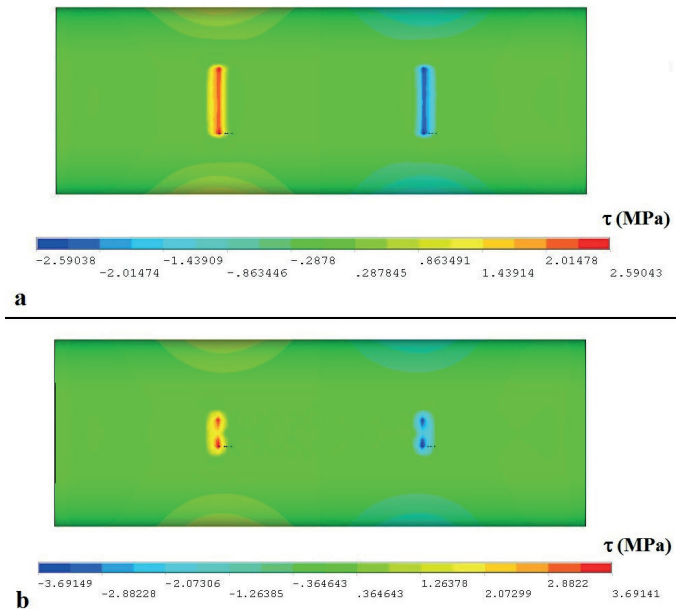


Fig. 15 Top views of shear stress distributions under 45° (a) and 25° (a) jaws

Depending on the shear strength and tensile strength values of the rock materials, 15° can be accepted as the ideal contact angle since the maximum shear stress induced in the case of 15° contact angle was found significantly higher than the tensile stresses.

As seen in Fig. 16, the location of the maximum tensile stress is downside surface at the middle length of specimen which contacts on the hole in the jaw, whereas the maximum shear is induced just beneath the edges of the middle block. Because the maximum shear and tension locations are different and distant from each other, the 15° jaw was found to have a significant advantage to make designation of the valid shear failure easy.

To check whether stress distributions vary with the change in different rock material properties like modulus of elasticity and Poisson's ratio, further material models were analysed. For the contact angle of 15°, $a = 3$ mm and $b = 60$ mm conditions,

Table 6 Maximum compressive stresses in different models

Loading Condition	Max. Compressive Stress (MPa)
$a: 3$ mm, $b: 20$ mm ($\alpha: 180^\circ$)	10.5
$a: 3$ mm, $b: 100$ mm ($\alpha: 180^\circ$)	10.0
$a: 0$ mm, $b: 60$ mm ($\alpha: 180^\circ$)	16.5
$a: 3$ mm, $b: 60$ mm ($\alpha: 180^\circ$)	16.2
$a: 6$ mm, $b: 60$ mm ($\alpha: 180^\circ$)	15.7
$a: 9$ mm, $b: 60$ mm ($\alpha: 180^\circ$)	15.0
$a: 3$ mm, $b: 60$ mm ($\alpha: 65^\circ$)	8.5
$a: 3$ mm, $b: 60$ mm ($\alpha: 45^\circ$)	11.1
$a: 3$ mm, $b: 60$ mm ($\alpha: 25^\circ$)	12.2
$a: 3$ mm, $b: 60$ mm ($\alpha: 15^\circ$)	20.1

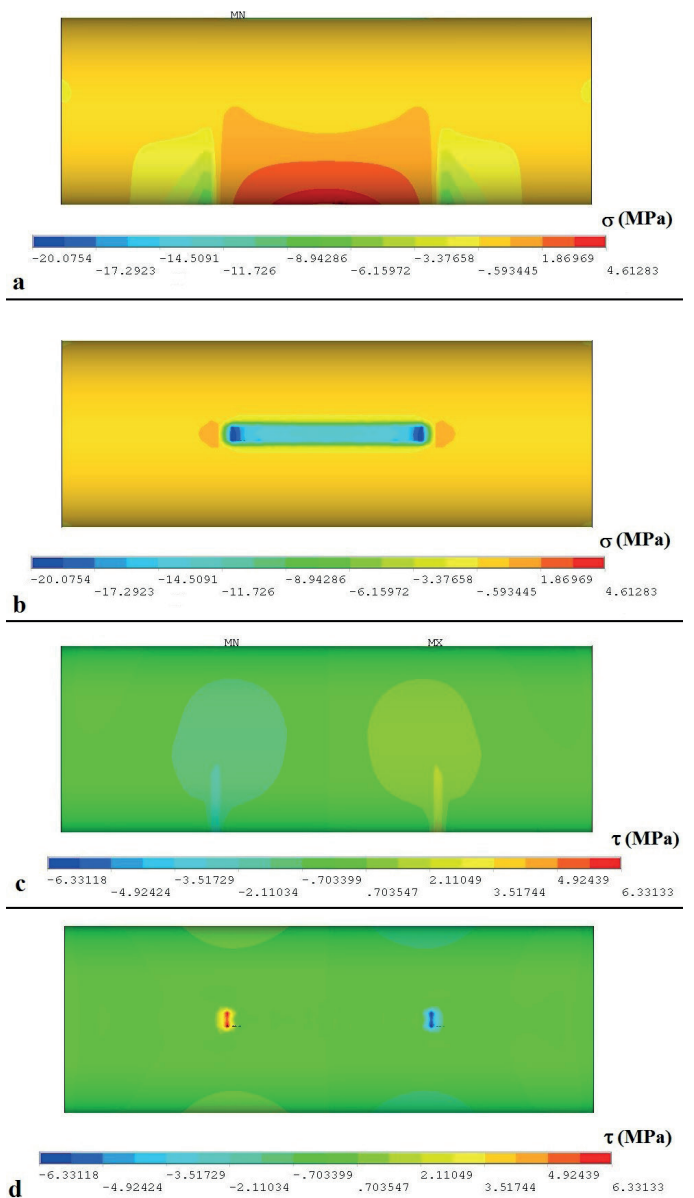


Fig. 16 Normal stress (a, b) and shear stress (c, d) distributions under 15° jaw (top views are given in b and d)

the formulation given in Eq. 1 was found convenient to estimate cohesion values from the failure load of the specimens. It should be noted herein that the Eq. 1 is only valid for the specimens having same dimensions with that analysed in this

study. The material properties of different rock models analysed for verifying the formulation between the maximum shear stress and failure load parameters are given in Table 7. Stress distribution details for different material models loaded under the contact angle of 15° can be seen in Table 8. As the relation between failure loads and shear strength values were similar for all the models, Eq. 1 including a coefficient interval from 1.52 to 1.66 was accepted to be usable for different rock materials modelled within this study (Table 7).

$$\tau_0 = (1.52-1.66)F_{max}/A \quad (1)$$

where τ_0 , F_{max} and A are respectively cohesion (MPa), maximum load (kN) and cross-section area of the core specimen (cm²).

4 Discussions and conclusions

Failure load variations with the change of loading conditions were found parallel in experimental and numerical modelling studies. This situation approves the representability of the numerical models for the experimental case. It was confirmed with the significant decrease of the failure load in case of being loaded under the condition of the high a values that the gap distance within the couple of shear forces should be limited to have a valid shear strength test failure by prevention of an effect improving the majority of tensile stresses which makes the early failure [11,12].

In contrast to the cement moulding method to hold specimens, use of the double shear jaw (DSJ) was seen to be a practical method to test numerous specimens by a cheap apparatus. Compared to the classical manual hydraulic shear strength test equipment, the new method is also advantageous because of having ability to load specimens with a constant rate. The classical shear strength test including cement moulding to hold specimens is generally restricted to only apply on low strength rock materials. On the other hand, it is possible to test both high strength and low strength rock materials by the use of DSJ.

In ideal failure shape, one shear crack which is parallel to the shear forces directions is formed and initiated due to the high shear stress concentrations instead of normal stresses [13–16]. With an increase in a value, tensile stress concentration at the maximum shear stress location was found to increase as an important disadvantage of big gaps between blocks (pieces) of the jaw. On the other hand, contacting blocks condition ($a = 0$ mm) has also some disadvantages making non-ideal failure shapes with frequent crack series and major crushing zones under high load values. To obtain the ideal simple crack shape, the gap condition of $a = 3$ mm was seen to be the most convenient selection investigated within this study. According to the results of this study, ideal b value was found to be 60 mm. As another geometric suggestion, the contact angle of the middle block of the DSJ should be 15° for a valid failure resulting from high shear stress concentrations instead of tensile stresses. In case of having no treatment of the middle block to decrease the contact angle, specimens were assessed to fail invalidly under the control of tensile stresses. Therefore, the hole treatment was found to be crucial.

The high load values, frequent cracks and crushing zone occurrence indicate the unnecessary and misleadingly high energy consumption values for the failure [17–19]. DSJs should be used carefully to determine the shear strength values of rocks by considering the failure validity. Considering the results of this study, it is possible to increase the shear stress concentration with a decrease in the contact angle. However, the significant increase in the compressive stresses should be taken into the account, as well. In terms of having a valid failure, the ratio of compressive strength to tensile strength values of tested rock materials must be high enough to have no crack initiation due to the reaching high compressive stress levels. The ratio of compressive strength to tensile strength typically varies between 8 and 15 for most of the rock materials [20–22]. The ratio between maximum compressive and

Table 7 Failure loads and their relation between maximum shear stress values for different material models loaded under 15° jaw and conditions of $a = 3$ mm, $b = 60$ mm (E = Modulus of Elasticity, ν = Poisson's ratio, F = Failure load, A is cross-section area of the core specimen that is about 2290 mm²)

Model	E (GPa)	ν	Failure Load, F (kN)	Max. Shear Stress, τ_{max} (MPa)	Equation
Material 1	30	0.25	9.18	6.33	$\tau_{max} = 1.58F/A$
Material 2	30	0.35	9.25	6.15	$\tau_{max} = 1.52F/A$
Material 3	30	0.15	8.47	5.91	$\tau_{max} = 1.60F/A$
Material 4	15	0.25	9.19	6.77	$\tau_{max} = 1.66F/A$
Material 5	45	0.25	8.76	5.86	$\tau_{max} = 1.53F/A$

Table 8 Shear stress and tensile stress relations for the models loaded under 15° jaw ($a = 3$ mm, $b = 60$ mm)

Model	Max. Shear Stress, τ_{max} (MPa)	Max. Tensile Stress, σ_{tmax} (MPa)	Equation
Material 1	6.33	4.61	$\tau_{max} = 1.4 \sigma_{tmax}$
Material 2	6.15	4.59	$\tau_{max} = 1.3 \sigma_{tmax}$
Material 3	5.91	4.56	$\tau_{max} = 1.3 \sigma_{tmax}$
Material 4	6.77	4.80	$\tau_{max} = 1.4 \sigma_{tmax}$
Material 5	5.86	4.65	$\tau_{max} = 1.3 \sigma_{tmax}$

maximum tensile stresses of 4 which was obtained for loading under the contact angle of 15° is found low enough for most of the rock materials for shear stress controlled failure made without reaching compressive strength values.

As another important point, the maximum shear stress induced in the tested material should be significantly higher than tensile stresses for valid shear failure. The contact angle of 15° was also found convenient considering typical relations between cohesion and tensile strength values of rock materials. Depending on rock materials and their mechanical properties, cohesion values can be higher or lower than the tensile strength values. As the maximum shear stress in the model loaded under 15° contact angle and the condition of $a = 3$ mm was determined to be nearly 40% higher than the maximum tensile stress, it is expected to see shear stress controlled crack initiation for most of the rock materials in case of testing under the condition [23,24].

The shear stress concentration was assessed to make failure of specimens in the use of 15° as confirmed by stress distribution obtained from the numerical analyses and failure mechanisms observed from the experimental study. Under the loading condition of 15° contact angle, it is a significant advantage to easily distinguish tensile and shear crack occurrences from failure shapes of the specimens. As confirmed by the numerical modelling, it is explicit to designate the invalid tensile failure resulting from the cracking at the middle length of specimens loaded under 15° jaw. Even though the invalid failure was not seen in the experimental study carried out using 15° jaw, it can be seen from tests of different rock materials, depending on the relation between tensile strength and cohesion values. DSJs should be carefully used to determine shear strength values of rock materials by considering to see the valid shape of shear failure initiated just beneath the edge of the treated hole. It should be reminded herein that observation of the typical and small spalling cracks beneath the edge of the treated hole is a verification of the shear stress induced failure.

The ratio between maximum shear and tensile stresses was found to increase with a decrease in the contact angle. As a desirable issue, shear stresses are significantly higher than tensile stresses under the loading condition of the small contact angles like 15°. However, the ratio of maximum compressive stress to maximum tensile stress values was found to also increase with the decrease in the contact angle values. Therefore, the use of jaws with quite small contacts like those of the line loading condition are not suggested to prevent reaching excessive compressive stress concentrations that can make invalid failures. In the use of 15° jaw, compressive stresses were not found to be enough high for causing the invalid compressive failure as the ratio of the maximum compressive stress was 4 times of the maximum tensile stress [25–27].

The novelty of this study is investigating the use of various contact angles instead of the full contact condition of conventional shear strength testing. Within different loading

conditions, the contact angle of 15° was found to make the ideal loading type. For the NX core size specimens loaded under the contact angle of 15°, $a = 3$ mm and $b = 60$ mm conditions, Eq. 1 is suggested to use in accordance with the results of this study. In short, use of the treated DSJs is suggested for determination of shear strength values of rock materials and assessed to have a good potential to be a popular test method in rock mechanics laboratories because of its practicality.

References

- [1] Ulusay, R., Hudson, J. A. "The blue book - the complete ISRM suggested methods for rock characterisation, testing and monitoring: 1974-2006". ISRM & Turkish National Group of ISRM, Ankara, 2007.
- [2] ASTM D5607-16: Standard Test Method for Performing Laboratory Direct Shear Strength Tests of Rock Specimens Under Constant Normal Force. ASTM International, West Conshohocken, PA (2016) <https://doi.org/10.1520/D5607-16>
- [3] Buocz, I., Rozgonyi-Boissinot, N., Török, A., Görög, P. "Direct shear strength test on rocks along discontinuities, under laboratory conditions". *Pollack Periodica*, 9(3), pp. 139–150. 2014. <https://doi.org/10.1556/Pollack.9.2014.3.15>
- [4] Ulusay, R., Gokceoglu, C., Binal, A. "Kaya Mekanigi Laboratuvarı Deneyleri". Chamber of Geological Engineers of Turkey, Ankara. 2005. (In Turkish)
- [5] Hackston, A., Rutter, E. "The Mohr–Coulomb criterion for intact rock strength and friction – a re-evaluation and consideration of failure under polyaxial stresses". *Solid Earth Journal*, 7, pp. 493–508. 2016. <https://doi.org/10.5194/se-7-493-2016>
- [6] Barton, N. "Shear strength criteria for rock, rock joints, rockfill and rock masses: Problems and some solutions". *Journal of Rock Mechanics and Geotechnical Engineering*, 5(4), pp. 249–261. 2013. <https://doi.org/10.1016/j.jrmge.2013.05.008>
- [7] Sarfarazi, V., Schubert, W. "Numerical Simulation of Tensile Failure of Concrete in Direct, Flexural, Double Punch Tensile and Ring Tests". *Periodica Polytechnica Civil Engineering*, 61(2), pp. 176–183. 2017. <https://doi.org/10.3311/PPci.9028>
- [8] Aziz, N., Pratt, D., Williams, R. "Double Shear Testing of Bolts". In: *Coal 2003: Coal Operators' Conference*, (Aziz, N. (Ed.)), University of Wollongong & the Australasian Institute of Mining and Metallurgy, pp. 154–161. 2003.
- [9] Komurlu, E., Cihangir, F., Turan, A., Kesimal, A., Erçikdi, B. "An Experimental Study on Shear Strength of Cemented Paste Backfill Materials". *Suleyman Demirel University Journal of Natural and Applied Sciences*, 22(1), pp. 45–52. 2017. <https://doi.org/10.19113/sdufbed.08547>
- [10] Willam, K. J., Warnke, E. P. "Constitutive model for the triaxial behaviour of concrete". *IABSE*, Report No. 19, Bergamo. pp. 1–30. 1974.
- [11] Kumbasar, N. "Betonarme Kesitlerin Eğilme Rijitliği". *IMO Teknik Dergi*, 26, pp. 7265–7278. 2015. http://www.imo.org.tr/resimler/dosya_ekler/6e16bda54af203e_ek.pdf?dergi=777
- [12] Alvarez Rabanal, F. P., Guerrero-Muñoz, J., Alonso-Martinez, M., Martinez-Martinez, J. E. "Bending and Shear Experimental Tests and Numerical Analysis of Composite Slabs Made Up of Lightweight Concrete". *Journal of Engineering*, 2016, Article ID 6819190. 2016. <https://doi.org/10.1155/2016/6819190>
- [13] Buocz, I., Rozgonyi-Boissinot, N., Török, Á. "Influence of Discontinuity Inclination on the Shear Strength of Mont Terri Opalinus Claystones". *Periodica Polytechnica Civil Engineering*, 61(3), pp. 447–453. 2017. <https://doi.org/10.3311/PPci.10017>

- [14] Barton, N., Shen, B. "Risk of shear failure and extensional failure around over-stressed excavations in brittle rock". *Journal of Rock Mechanics and Geotechnical Engineering*, 9(2), pp. 210–225. 2017.
<https://doi.org/10.1016/j.jrmge.2016.11.004>
- [15] Luo, Y., Wang, T. H., Liu, X. J., Zhang, H. "Laboratory Study on Shear Strength of Loess Joint". *Arabian Journal for Science and Engineering*, 39(11), pp. 7549–7554. 2014.
<https://doi.org/10.1007/s13369-014-1318-x>
- [16] Hasanpour, R., Choupani, N. "Rock fracture characterization using the modified Arcan test specimen". *International Journal of Rock Mechanics and Mining Sciences*, 46(2), pp. 346–354. 2009.
<https://doi.org/10.1016/j.ijrmms.2008.07.004>
- [17] Komurlu, E., Kesimal, A. "Evaluation of Indirect Tensile Strength of Rocks using Different Types of Jaws". *Rock Mechanics and Rock Engineering*, 48, pp. 1723–1730. 2015.
<https://doi.org/10.1007/s00603-014-0644-3>
- [18] Komurlu, E., Kesimal, A., Demir, S. "Experimental and Numerical Study on Determination of Indirect (Splitting) Tensile Strength of Rocks under Various Load Apparatus". *Canadian Geotechnical Journal*, 53(2), pp. 360–372. 2016.
<https://doi.org/10.1139/cgj-2014-0356>
- [19] Komurlu, E., Cihangir, F., Kesimal, A., Demir, S. "Effect of adhesive type on the measurement of elasticity modulus using electrical resistance strain gauges". *Arabian Journal for Science and Engineering*, 41(2), pp. 433–441. 2016.
<https://doi.org/10.1007/s13369-015-1837-0>
- [20] You, M. "Strength criterion for rocks under compressive-tensile stresses and its application". *Journal of Rock Mechanics and Geotechnical Engineering*, 7(4), pp. 434–439. 2015.
<https://doi.org/10.1016/j.jrmge.2015.05.002>
- [21] Perras, M. A., Diederichs, M. S. "A Review of the Tensile Strength of Rock: Concepts and Testing". *Geotechnical and Geological Engineering*, 32(2), pp. 525–546. 2014.
<https://doi.org/10.1007/s10706-014-9732-0>
- [22] Komurlu, E., Kesimal, A., Demir, A. D. "Dogbone shaped specimen testing method to evaluate tensile strength of rock materials". *Geomechanics and Engineering*, 12(6), pp. 883–898. 2017.
<https://doi.org/10.12989/gae.2017.12.6.883>
- [23] Konietzky, H., Ismael, M. "Failure Criteria for Rocks – an Introduction". In: *Introduction into Geomechanics*, (Gribsch, A. (Ed.)), Geotechnical Institute TU Bergakademie Freiberg. 2017.
- [24] Karakul, H., Ulusay, R. "Kayaların Dayanım Özelliklerinin Farklı Doygunluk Koşullarında P-dalga Hızından Kestirime P-Dalga Hızının Fiziksel Özelliklere Olan Duyarlılığı". *Yerbilimleri*, 33(3), pp. 239–268. 2012.
- [25] Briševac, Z., Kujundžić, T., Macenić, M. "Estimation of Uniaxial Compressive and Tensile Strength of Rock Material from Gypsum Deposits in the Knin Area". *Tehnički Vjesnik*, 24(3), pp. 855–861. 2017.
<https://doi.org/10.17559/TV-20150130152828>
- [26] Coviello, A., Lagioia, R., Nova, R. "On the Measurement of the Tensile Strength of Soft Rocks". *Rock Mechanics and Rock Engineering*, 38(4), pp. 251–273. 2005.
<https://doi.org/10.1007/s00603-005-0054-7>
- [27] Karakul, H., Ulusay, R. "Empirical Correlations for Predicting Strength Properties of Rocks from P-Wave Velocity under Different Degrees of Saturation". *Rock Mechanics and Rock Engineering*, 46(5), pp. 981–999. 2013.
<https://doi.org/10.1007/s00603-012-0353-8>